Plasmon excitations in quasi-one-dimensional $K_{0.3}MoO_3$

M. Sing, V. G. Grigoryan, G. Paasch, M. Knupfer, and J. Fink
Institut für Festkörper- und Werkstofforschung Dresden, D-01171 Dresden, Germany

B. Lommel* and W. Aßmus
Physikalisches Institut, Universität Frankfurt, D-60054 Frankfurt, Germany

(Received 23 July 1998)

We present an investigation of the plasmon excitations in a quasi-one-dimensional metal, the blue bronze $K_{0.3}MoO_3$. The dispersion relation along the one-dimensional direction, as measured by electron energy-loss spectroscopy in transmission, is quasilinear over a wide momentum range before it exhibits a negative curvature. We show that the quasilinear part can be explained within an essentially three-dimensional model based on the random-phase approximation. Band-structure effects are thereby considered through the Ehrenreich-Cohen formula, tailor-made to the specific, strongly anisotropic material. From this analysis, we find no hint for exceptional properties caused by one dimensionality as is currently discussed in the context of photoemission measurements. The genuine dependence of the plasmon modes on the propagation angle relative to the one-dimensional axis is masked by interband transitions lying at about the same energy as the plasmon excitations itself. [S0163-1829(99)00508-1]

I. INTRODUCTION

The fundamental theory for the description of the low-lying excitations in an interacting many-electron system is the well-known concept of a normal Fermi liquid (FL).[1] For example, it elucidates why it is possible to explain the electronic properties of an ordinary metal essentially within a one-particle picture despite the strong electron-electron Coulomb repulsion. The underlying idea consists in the one-to-one correspondence between the bare electron states of the noninteracting and the dressed or quasiparticle states of the interacting system, which may thus be viewed as composed of independent particles with renormalized mass. This basic concept can be extended to cases where the systems in question do not obey this definition and its implications in a strict sense, such as for metals that become superconducting.[2] One then omits the epithet ''normal'' and simply speaks of a FL. On the other hand, the applicability of the FL theory to the two-dimensional (2D) cuprate high-temperature superconductors both in the normal and the superconducting state has been discussed controversially and is still an open question.[3,4] This illustrates that although the FL theory in general has turned out to be quite robust and flexible and may be applied widely its applicability in each specific case may be the subject of subtle considerations. Thus, the FL theory can be regarded as setting a standard in condensed matter physics by classifying both real and model systems as normal, i.e., showing FL, versus extraordinary, i.e., showing non-FL behavior.

On the theoretical side, however, there is a paradigm for which the failure of the FL picture is unambiguous, namely in the model system of interacting electrons, which are restricted in their motion to only one dimension. The breakdown of the FL theory in one dimension originates from the logarithmic divergence of the particle-hole susceptibility at the wave vector $2k_F$ (k_F being the Fermi momentum) due to the ideal nesting property of a 1D Fermi surface.[5] One way to deal with this Peierls instability is via the opening of a Peierls gap if an adiabatical coupling of the electrons to the phonons is taken into account. This approach results in the occurrence of a metal-insulator transition due to the formation of a charge-density wave (CDW) connected with a static lattice distortion.

Another possible approach is based on the consideration of the electron-electron correlations alone while the electron-phonon interactions are neglected. This route is followed by the Tomonaga-Luttinger model (which can be solved exactly),[6–8] and the generalization thereof to other gapless 1D quantum systems characterized by the same universal low-energy phenomenology led to the notion of a Luttinger liquid (LL).[9] A striking property of the LL as opposed to a FL is the occurrence of bosonic collective modes, involving spin-charge separation instead of the fermionic quasiparticles.[10]

Whereas the phonon-driven CDW phase transition outlined above, as well as the resulting groundstate have been intensively studied in various compounds and may be considered as essentially fully understood,[11] renewed interest from the viewpoint of the LL approach has been attracted by crystalline realizations of 1D systems, such as the so-called blue bronze $K_{0.3}MoO_3$ or $(TaSe_4)_2I$.[12–15] From photoemission measurements of these systems, a suppression of spectral weight at the Fermi level E_F together with a redistribution of spectral weight to higher binding energies reaching up to about 0.5 eV below E_F was reported. This was dicussed as being a possible signature of LL behavior because this observation contradicts the expectation of a clear Fermi cutoff as is characteristic for metals in two or three dimensions. Much effort has been spent both to confirm these experimental findings also on other materials,[16–19] and to gain more theoretical insight into this question.[20–24] Although the experimental phenomenon as described above may be thought to be well established for various compounds, it is fair to say that there is a growing opinion that there exists no

 ©1999 The American Physical Society

unique cause for this suppression of spectral weight at E_F common to all these systems. However, the basic question is how far the specific LL phenomenology persists at all in real crystal systems where one necessarily deals with 1D chains coupled to each other via the Coulomb interaction and electron hopping, the latter of which, strictly speaking, makes the system a FL instead of a LL. As far as the one-particle spectral function is concerned, to which photoemission spectroscopy (PES) is suited to give direct access, this issue has been further explored. It was concluded that there should be an intermediate regime with respect to energy and momentum where the universal features of a LL should persist and be observable with spectroscopic techniques such as PES.[24] However, up to now, neither the qualitative predictions such as spinon and holon excitations reflecting the above-mentioned spin-charge separation, nor the quantitativley exploitable ones, like the power-law behavior of the spectral function in the vicinity of the Fermi level,[24] could be verified experimentally beyond doubt.

Moreover, little attention has been paid in the course of the current discussion to other spectroscopic methods, which probe other response functions. This applies, for example, to measurements of the dc conductivity where the experimental data for various compounds, among them also the blue bronze, could be explained satisfactorily on the basis of the quasiclassical Boltzmann equation utilizing solely the temperature dependent pseudogap as a specific 1D feature.[25,26] A further quantity of particular interest are the plasmon modes, which can be measured as sharp peaks in the frequency and momentum-dependent loss function. This in turn is related to the two-particle Green's function (GF), whereas the spectral function widely studied up to now is connected to the one-particle GF. The plasmon dispersion is known to be a sensitive probe of electron correlation effects, and is hence especially suited in this context, since these effects are the fundamental reason for the above-mentioned breakdown of the FL picture in one dimension.

Measurements of the plasmon dispersion in the context of quasi-one-dimensional conducting compounds have been reported up to now only for the organic charge-transfer salt TTF-TCNQ,[27] for polymeric $(SN)_x$,[28] and recently for the transition metal tetrachalco-halogenide $(TaSe_4)_2I$.[29] For the latter compound, a quasilinear plasmon-dispersion relation over a wide momentum range for the direction parallel to the 1D axis was found. This behavior could be understood in terms of band-structure effects, treated on the level of the random-phase approximation, in agreement with existing tight-binding (TB) band-structure calculations. In the case of the TTF-TCNQ, the measurements suffered from the twinning of the crystals by an angle of 90°. Only if one assumes (unrealistically) a vanishing transverse hopping probability $t_\perp$ between neighboring chains, the plasmon energy for the direction perpendicular to the 1D direction would become zero and its spectral weight would vanish.[30] Otherwise, the only unique direction that could be measured for TTF-TCNQ is the direction with a plasmon propagation angle of 45° relative to the 1D direction. There, within the error bars, a more or less constant plasmon energy with increasing momentum transfer was observed. Interestingly, theoretical models, which were developed or adapted to account for the experimental data on TTF-TCNQ, could satisfactorily explain the plasmon dispersion as measured nominally parallel to the 1D direction but failed in describing the experimental findings for a propagation angle of 45°.[31,32] These models were both based on the RPA, one of which also included corrections for exchange.[32] However, none of them properly described the interchain coupling since only the mutual Coulomb interaction was considered in the calculations.

We do not dicuss here the results on $(SN)_x$ further since one of the conclusions of this study[28] was that this system should not be considered as 1D but rather as 2D or 3D. This was also concluded from other measurements and is meanwhile generally accepted.[33] Instead, we refer to this study regarding the attempt made therein to derive the angular dependence of the plasmon energy at zero momentum transfer from measurements of the optical reflectance of the mixed-valence platinum complex compound $K_2Pt(CN)_4Br_{0.3}0.3H_2O$ (Ref. 34) and TTF-TCNQ.[35] In these reflectivity studies the real and imaginary part of the dielectric function were derived by means of a Kramers-Kronig analysis for the directions parallel and perpendicular to the 1D directions. The zero crossing of the real part of the dielectric function was then calculated in Ref. 28 as a function of the propagation angle according to $\varepsilon_\parallel \cos^2(\theta)+\varepsilon_\perp \sin^2(\theta) =0$ to give the plasmon energy. A $\cos\theta$ dependence for the plasmon energy was thereby arrived at, as predicted from all theoretical models neglecting the interchain coupling as far as mediated by a finite transverse electron-hopping probability.[32,36–39] Although this procedure may be regarded as a reasonable attempt to extract some information from the optical data, it is by no means a direct probe of the angular dependence of the plasmon modes which, in any case, cannot be excited by transverse electromagnetic waves, i.e., in an optical experiment.

To close the circle with respect to the present discussion concerning possible LL behavior in quasi-one-dimensional systems we note that also in a LL-based description the $\cos(\theta)$ angular dependence of the plasmon energy for $q\rightarrow 0$ holds for a zero transverse hopping probability.[10,40] However, for plasmon excitations parallel to the 1D direction, under the inclusion of at least the Coulomb interaction as coupling the 1D chains to each other, no calculations are available to our knowledge. Omitting such a 3D coupling leads to an acoustical plasmon branch.[41] A LL treatment including finite $t_\perp$ and for finite momentum transfers, however, poses difficult problems and unfortunately remains to be carried out. However, since a renormalization of the Fermi velocity is expected from theoretical considerations,[10,41] one can conceive of seeing manifestations thereof also on the energy scale of the plasmon excitations, and especially expressed in the plasmon dispersion.

Therefore, we present measurements of the plasmon dispersion in the blue bronze, which is currently discussed as being outstanding in terms of possible LL behavior, using electron energy-loss spectroscopy (EELS) in transmission. We have measured both along the chain direction and as a function of the angle relative to the 1D direction and explain quantitatively the quasilinear part of the plasmon dispersion parallel to the 1D direction by developing out a model based on the well-established RPA. We find no evidence for any

unique feature that would suggest the need for a treatment within the framework of a LL.

II. EXPERIMENT

The $K_{0.3}MoO_3$ single crystals were grown from fused salt mixtures of K_2MoO_4 and MoO_3 by electro crystallization.[42] Characterization and orientation of the crystals were carried out by means of x-ray diffraction and polarization-dependent reflectance measurements in the UV/vis. Free-standing thin films with a thickness of about 1000 Å, as suitable for EELS measurements, were cut using an ultramicrotome equipped with a diamond knife. While *in situ* electron diffraction spectra along the 1D direction, i.e., the crystallographic *b* axis, showed only resolution-limited widths of the Bragg reflections (thus indicating that in this direction the crystallinity was hardly affected) for the direction perpendicular to it, i.e., the crystallographic [102]-direction,[43] some broadening and mosaic spread could be observed, which is an expected consequence of the folding of the film due to the cutting procedure with the knife edge aligned parallel to the chains. The degree of chain orientation, as determined by the full width at half maximum of the (020) reflection as a function of the polar and azimuthal angle, was typically about 2.5° and 3.5°, respectively. The crystal symmetry is side-centered monoclinic, space group $C2/m$, with the lattice parameters $a=18.249$ Å, $b=7.561$ Å, $c=9.856$ Å, and $\beta=117.54°$ at 300 K.[43–45] To correlate the above-mentioned crystallographic directions, with the real structure of the blue bronze, we just note that the structure can be viewed as being an arrangement of clusters, each of them built up of ten edge sharing MoO_6 octahedra in such a way that these subunits are joined by corners in two directions, and thus basically form infinite sheets, which are separated by the K ions. However, while in the 1D direction the number of common corners between the subunits is four, there are only two in the in-plane direction perpendicular to it.[43] This structural anisotropy is reflected, for instance, both by measurements of the dc conductivity,[25,26] which give an anisotropy ratio of 1:10:100 for the direction perpendicular to the sheets, the in-plane direction perpendicular to the chain direction, and the 1D chain direction itself, respectively, and also by the occurrence of a Peierls transition at 183 K[46] into a CDW ground state. The transmission EELS measurements were performed at room temperature with a purpose-built spectrometer.[47] The loss spectra were recorded with an energy and momentum resolution of 115 meV and 0.05 $Å^{-1}$, respectively.

III. THEORETICAL CONSIDERATIONS

Plasmon excitations in the context of organic and inorganic quasi-one-dimensional metals have been considered quite comprehensively by Williams and Bloch[36] within the random-phase approximation (RPA). They treated a square array of 1D chains, coupled to each other only by the Coulomb interaction, assuming a *model* electron spectrum for two extreme cases, namely the limits of free and of tightly bound electrons constrained to a first-nearest-neighbor hopping within the chains. Hence, in their calculations of the dielectric function and the plasmon dispersion only *normal intraband* transitions were taken into account. The spatial inhomogeneity of the electron distribution along and perpendicular to the chains, known as crystal local-field effects, was incorporated in a simplified manner. Our attempts to explain the experimental plasmon dispersion in the one-dimensional conductor $K_{0.3}MoO_3$ applying these model calculations were unsuccessful, as we did not achieve a satisfactory agreement fitting the theoretical plasmon curves for either of the extreme cases to our experimental data. As in the case of $(TaSe_4)_2I$[29] we are, therefore, led to analyze the observed plasmon dispersion in the blue bronze by accounting adequately for the *real* electronic transitions, i.e., *normal and umklapp intra-/interband* transitions, while wanting to stay within the framework of the RPA. The RPA is well known to be applicable in three dimensions for the long-wavelength regime at high-electron densities, but a point that is less established is that it is an even better approach in one dimension if one follows recent studies.[48,49] Nevertheless, in one dimension the RPA, being a prototypical example of a standard FL-type electron gas theory, is in competition with a description based on a LL scenario. However, the latter has not been treated theoretically up to now with respect to the plasmon excitation modes for our case of a quasi-one-dimensional electron system represented by coupled 1D strands.[10,40,41] We deliberately desist from the inclusion of both a proper treatment of the crystal local-field effects and of corrections for exchange[32,37,38,50,51] and correlation[37,51,52] to the RPA in order to bring into sharper focus the main physical processes controlling the observed plasmon dispersion in this compound.

A. Electronic spectrum of $K_{0.3}MoO_3$

The unit cell of the blue bronze contains 20 f.u., i.e., 86 atoms, which make it currently beyond the reach of full band-structure calculations based on the local-density approximation within the density-functional theory. The existing TB band-structure calculations by Travaglini and Wachter[53] and Whangbo and Schneemeyer,[54] however, disagree with one another both in the form of the Fermi surface and in the conduction band width. For instance, according to Ref. 53 the width of the conduction-band is ≈ 1 eV, whereas it is only ≈ 0.3 eV in Ref. 54.

We favor the band-structure model of Travaglini and Wachter—and hence base our considerations upon it—for the following reasons: (i) many quantities calculated on the basis of this model, such as the optical effective mass, the mean-field effective mass for the oscillatory motion of the pinned CDW below the Peierls temperature, and the dc conductivity, as well as the conduction-band width itself agree quite well with the available optical[55,56] and dc electrical transport[25] data. (ii) X-ray photoemission spectroscopy shows a conduction band extending about 2 eV below the Fermi level with strong Mo 4*d* character,[57] which is in line with the model of Travaglini and Wachter, particularly in connection with (iii) recent results obtained by angle-resolved photoemission spectroscopy,[57,58] where two conduction-band features could be observed, which disperse by about a factor of 2 and 5 more strongly than the bands calculated in Ref. 54. (iv) The TB band structure of Travaglini and Wachter is also consistent with the results of core-

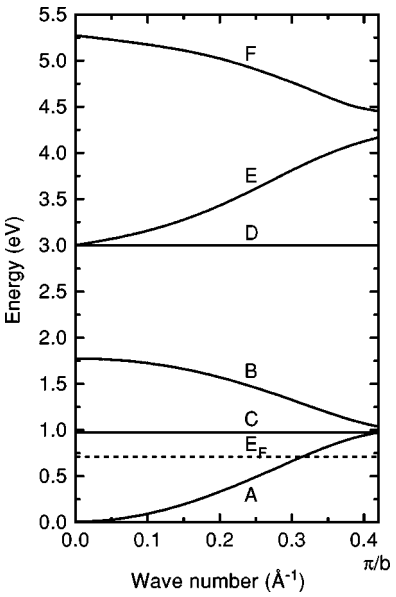

FIG. 1. Band structure of $K_{0.3}MoO_3$ according to Ref. 53.

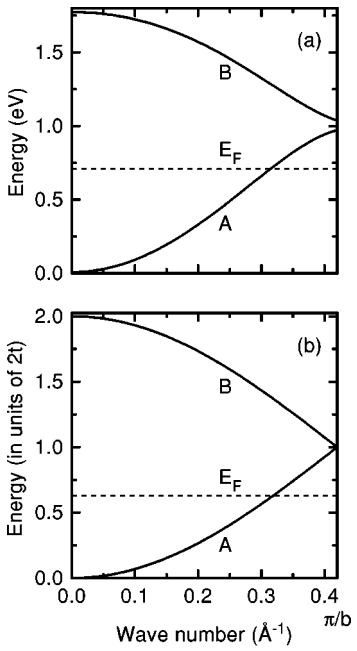

FIG. 2. (a) Band structure of $K_{0.3}MoO_3$ in the vicinity of the Fermi energy E_F according to Ref. 53. (b) Model band structure for the blue bronze according to Eq. (1) of this work. For details see the text.

level excitation spectra recorded by means of x-ray absorption spectrocopy, which probe the unoccupied part of the electronic structure.[59]

The results of the TB calculation of Travaglini and Wachter performed for a single cluster chain of $K_{0.3}MoO_3$ are shown in Fig. 1 (solid lines). The conduction-band A has t_{2g} character and is three-quarters filled by the $4s$ electrons transferred from the K atoms. This gives a Fermi wave number $k_F=(3/4)(b^*/2)$, where $b^*=2\pi/b$ is the primitive reciprocal lattice vector parallel to the z direction. Additionally to the spin degeneracy, the conduction band is doubly degenerate because there arise two bands due to the overlap between the degenerate Mo d_{xz} and Mo d_{yz} orbitals. The upper band B results approximately from the back folding of the conduction band if one omits the small gap of about 0.1 eV at the boundary of the first Brillouin zone (BZ). In between the bands A and B is situated a nondispersive band C, which is derived from the Mo d_{xy} orbital. Ideally, this band does not couple for symmetry reasons to the bands A and B, and hence, from this point of view, does not give any contribution to the dielectric function along the z direction $\varepsilon(q_z,\omega)$, in the range of the plasmon energy. The minimal energy separation of all other bands (D,E, and F) from the Fermi energy is about 2.3 eV, and thus is sufficiently large compared to the maximal plasmon energy of about 1.9 eV, to mean that these other bands give only a small contribution to the dielectric function, and therefore can be neglected in this context. Consequently, only the bands A and B are important for our objectives.

To proceed, we parametrize the conduction-band A and the band B using the ansatz

$$E^A_{k_z}=2t[1-\cos(k_z b/2)], \quad E^B_{k_z}=2t[1+\cos(k_z b/2)], \tag{1}$$

which reflects well the main features of the electronic spectrum discussed above: i.e., the nearly identical symmetry of the bands A and B and the folded band structure. The agreement is evident from the representation of these two bands in Fig. 2(b) compared with the TB results in Fig. 2(a). Obviously, Eqs. (1) do not account for the small gap of ~ 0.1 eV at the edge of the BZ, but the influence of that gap on the plasmon dispersion is negligibly small since the minimal plasmon energy of about 1.5 eV is significantly larger.

Since the boundaries of the first BZ are situated at $\pm b^*/2=\pm 0.42$ Å^{-1} and the 1D Fermi wave number is $k_F=0.31$ Å^{-1}, already for $q_z>0.1$ Å^{-1} umklapp processes play a role. Thus, the possible electronic transitions, which give rise to the plasmon spectrum are (i) normal and umklapp intraband transitions $A\rightarrow A$ and (ii) normal and umklapp interband transitions $A\rightarrow B$. In Fig. 3(a) these different kinds of electron transitions are marked exemplarily by arrows within the repeated-zone scheme for the electronic structure. In Appendix A, exploiting Bloch's theorem, we show in detail that due to the folded structure of the bands A and B both normal interband transitions $A\rightarrow B$ and umklapp intraband transitions $A\rightarrow A$ are forbidden [dotted arrows in Fig. 3(a)]. Since umklapp interband transitions appear as normal intraband transitions in the extended-zone scheme [see Figs. 3(a) and 3(b)] it is possible, and actually more convenient, to carry out the calculations in this representation considering only normal intraband transitions within a single band, denoted by A_0 in Fig. 3(b) (the allowed transitions are depicted by solid arrows in Fig. 3). The zone boundaries then lie at $\pm b^*=\pm 0.84$ Å^{-1}.

B. Plasmon dispersion in $K_{0.3}MoO_3$ for long wavelengths

The plasmon excitation is determined by the zero of the real part of the dielectric function

$$0=\varepsilon_1(\mathbf{q},\omega)\approx\varepsilon_\infty-\frac{4\pi e^2}{q^2}\frac{2}{(2\pi)^3}\int d^3k\frac{2f(E_\mathbf{k})\Delta E_{\mathbf{k},\mathbf{q}}}{(\hbar\omega)^2-(\Delta E_{\mathbf{k},\mathbf{q}})^2}, \tag{2}$$

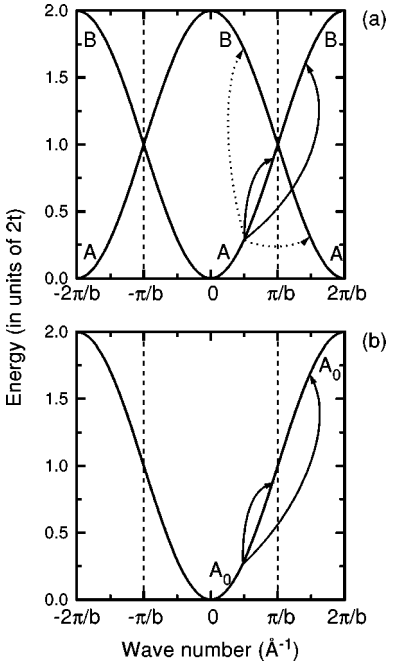

FIG. 3. (a) Bands *A* and *B* in the repeated-zone scheme. The possible electronic transitions are marked by arrows. Solid arrows indicate allowed and dotted ones forbidden transitions. (b) The same bands as in (a) plotted in the extended-zone scheme and now denoted as one band A_0. Only the respective allowed transitions are depicted as arrows. For details see the text.

where f is the Fermi distribution function and $\Delta E_{\mathbf{k},\mathbf{q}}=E_{\mathbf{k}+\mathbf{q}}-E_{\mathbf{k}}$ is the intraconduction-band excitation energy for a momentum transfer $\mathbf{q}$. In Eq. (2) we use the 3D Ehrenreich-Cohen expression[60] for the dielectric function, but take into account the 1D nature of the conduction band. Contributions to the dielectric function from high-energy interband transitions and core-level transitions are described by a background dielectric constant ε_∞. As explained above, we include in the dielectric function only the normal intraband transitions from the band *A* to the defolded band *B*. We are aware of the influence of the additional modulation of the electron density by the lattice. The lack of any ansatz for the wave functions underlying the above-cited band-structure calculations excludes a consistent treatment of these effects. However, this is a tolerable deficiency since a simple estimation gives a wave number of $q_z<b^*/2=\pi/b=0.42$ Å^{-1} as a limit below which these effects should be of little importance.

The long-wavelength plasmon dispersion is given by

$$\omega(\mathbf{q})=\omega_p+Aq^2, \quad A=\frac{\hbar}{m}\alpha, \tag{3}$$

where usually instead of the experimental dispersion coefficient A the dimensionless quantity α is introduced. In its definition the free-electron mass m is used to avoid confusion due to the existence of different notions of effective masses. For the special 1D electron spectrum (1) considered here one obtains (as developed in Appendix B) in the long-wavelength limit

$$\omega_p^2=\frac{16e^2N_0|v_F|}{\varepsilon_\infty\hbar}, \tag{4}$$

$$\alpha=\alpha_1+\alpha_2 \quad \text{with} \quad \alpha_1=\frac{mv_F^2}{2\hbar\omega_p}$$

and

$$\alpha_2=-\frac{me^2N_0b^2v_F}{6\hbar^2\varepsilon_\infty\omega_p}, \tag{5}$$

$$v_F=\frac{1}{\hbar}\left(\frac{\partial E_{k_z}}{\partial k_z}\right)_{k_F}=\frac{bt}{\hbar}\sin\left(\frac{k_Fb}{2}\right), \tag{6}$$

where v_F is the Fermi velocity and $N_0=2/(ac\sin\beta)$ is the number of cluster chains per surface unit of the x-y plane. A detailed discussion of the physical origin of α_1 and α_2 in terms of quasiclassical electron dynamics is reserved for a future publication in connection with the plasmon dispersion in the alkali metals.[61] Here we merely summarize the main results. The coefficient α_1 is connected with the deformation potential and is always positive, irrespective of the band structure, since the local changes of the density for finite wavelength increase the restoring force on a single electron, and hence the frequency of the collective charge oscillation, i.e., the plasmon. On the other hand, α_2 is determined by the derivative of the reciprocal dynamic effective mass at the Fermi energy. Evidently, this term vanishes for a free-electron-like or parabolic band. That the contribution of α_2 is by no means negligible, although it has been overlooked in the literature so far, is strikingly demonstrated for the alkali metals, especially for Cs, where despite only a small deviation of the conduction band from a parabolic form α_2 leads to a negative dispersion as observed experimentally.[62] In our case, inserting the values determined below, the ratio $\alpha_1/\alpha_2\approx-5$, which again emphasizes the importance of α_2.

IV. RESULTS AND DISCUSSION

A. Plasmon excitations parallel to the chain direction

In Fig. 4 we show a series of energy-loss spectra recorded along the one-dimensional direction for different momentum transfers. The curves are normalized to a feature between about 5.5 and 7 eV (not shown) whose intensity is independent of q as is asserted by a correction of the intensities for the $1/q^2$ dependence of the double differential cross section. For the lowest momentum transfer, i.e., 0.08 Å^{-1}, a considerable contribution from the direct beam centered at zero-energy loss is visible, which results from the finite momentum resolution and its broadening due to quasielastic scattering. This poses a lower boundary for the experimentally accessible momentum transfers. In the energy region shown, one clearly sees a dispersive peak, which is related to the plasma oscillation of the free charge carriers located in the two degenerate bands crossing the Fermi level along the metallic 1D direction. Although the plasmon peak gets broader, even at the highest measured momentum transfer of 0.625 Å^{-1} one can still speak of a well-defined though strongly damped plasmon excitation. However, at such high momentum transfers a reliable determination of the energy

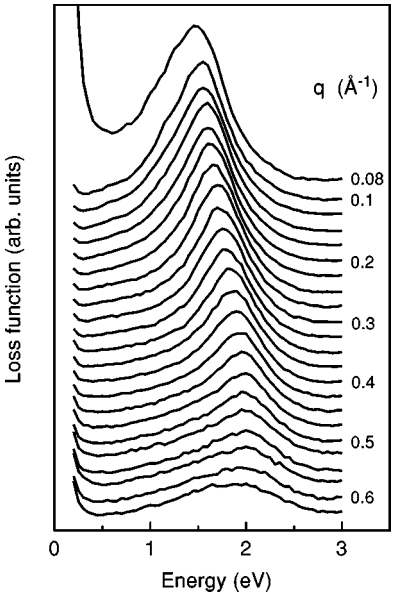

FIG. 4. Normalized electron energy-loss spectra of $K_{0.3}MoO_3$ for different momentum transfers along the 1D direction. The spacing in momentum transfer between the unlabeled curves is 0.025 $Å^{-1}$.

position becomes increasingly difficult and—also because of the reduced cross section—this value of 0.625 $Å^{-1}$ may be regarded as a reasonable upper boundary for the momentum range measurable using EELS.

A closer look at the behavior of the plasmon width as a function of momentum transfer is imparted by Fig. 5. The peak widths were determined by fitting the shape of the plasmon spectral feature with a model loss function incorporating, besides the Drude part, also a contribution from a Lorentz oscillator with small oscillator strength, which is necessary to achieve a good fit for the higher energy tail. Such a model function, of course, is physically justified only for zero momentum transfer. However, basically any suitable fit function could be used instead, and our particular choice is led by optical reflectivity measurements where a shoulder is seen in the plasma edge, which may be assigned in a simple molecular energy-level scheme to $\pi^* \rightarrow \pi^*$ interband

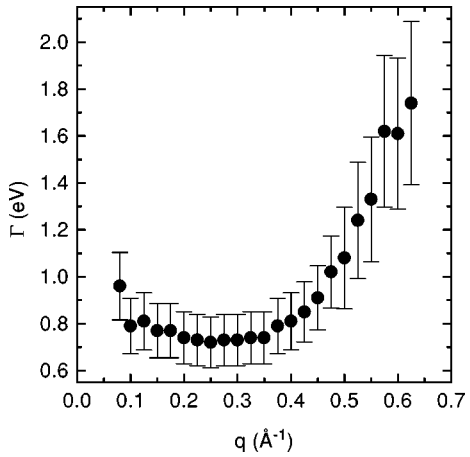

FIG. 5. Plasmon width (in eV) as a function of momentum transfer (in $Å^{-1}$) along the 1D direction as derived from the spectra shown in Fig. 4.

transitions (where the π^* states are formed by hybridization of the Mo $4dt_{2g}$ orbitals with the surrounding oxygen orbitals[56]) or, to remain in the picture of the TB band structure of Fig. 1, to transitions involving band *C* and to normal interband transitions $A \rightarrow B$ which both, realistically, may not be *entirely forbidden* for symmetry reasons as argued in the context of the derivation of our model band structure (which disregards the small gap of about 0.1 eV at the zone boundary of the first BZ) in Sec. III A, but only *strongly suppressed*. Due to the lower energy resolution in EELS, no signature of these interband transitions is discernible in the loss function, apart from the need of an additional oscillator for the fitting as mentioned above.

From this procedure, a region of a more or less constant width of about 0.73 eV in a momentum transfer interval between 0.15 and 0.35 $Å^{-1}$ can be extracted. For higher momentum transfers a steep continuous increase in the plasmon width is observed, while for the few values at momentum transfers lower than 0.15 $Å^{-1}$ only a tendency towards a slightly higher width can be seen. In a one-dimensional system the plasmon does not enter the continuum of excitations of electron-hole pairs with increasing momentum transfer as is the case in two or three dimensions.[49] This means that the plasmon damping mechanism, which is effective above a critical wave vector, known as Landau damping, is absent. Hence, the plasmon decay in the blue bronze should take place mainly through decay channels involving interband transitions, provided that the transverse interchain coupling resulting from the wave-function overlap is small. Thus, a quantitative explanation of the observed plasmon damping demands quite a detailed knowledge of these excitation processes, i.e., about the joint density of states and the transition matrix elements, and hence is beyond the scope of this paper. Nevertheless, the slightly increased width of the plasmon feature for the lowest momentum transfers may be ascribed to surface contributions, whose cross section scales with $1/q^3$, or to stronger contributions from the direct beam, both of which would broaden the observed plasmon width at low q.

The discussion so far raises a crucial question that has to be clarified before one can continue with an analysis of the experimentally observed plasmon dispersion in terms of the theoretical approach developed above. It is well known and easily demonstrated within a simple Drude-Lorentz model that the (Drude-)plasmon and a Lorentz-oscillator, which represents any other electronic excitation, may influence each other in a complex way in the loss function if they are not separated enough in energy. Simply put, they tend to repel each other.[47] Thus, one has to make sure in a more precise manner than provided by the argument given earlier that the oscillator strength of the $\pi^* \rightarrow \pi^*$ interband transitions is such that their impact on the plasmon dispersion can indeed be neglected, i.e., that they only lead to a broadening of the observed plasmon signature as stated above. Moreover, only if these interband transitions are weak does it make sense to introduce a background dielectric constant ε_∞, which is truly not frequency dependent in the energy region of interest, as is done in our theoretical approach. To address these points, we performed a Kramers-Kronig analysis (KKA) to obtain the absolute value of the loss function and the real and imaginary part of the dielectric function as

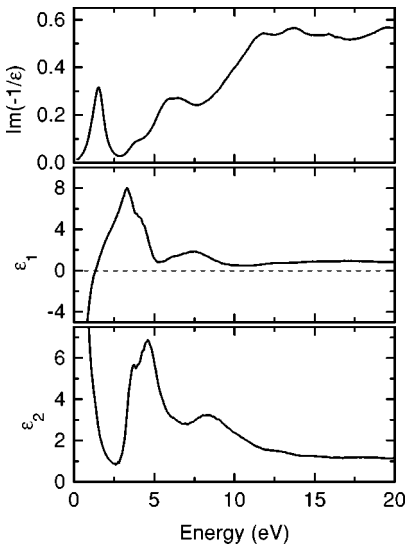

FIG. 6. The loss function $\mathrm{Im}(-1/\varepsilon)$ and the real (ε_1) and imaginary part (ε_2) of the dielectric function of $K_{0.3}MoO_3$ for a momentum transfer of $q=0.1$ Å^{-1} along the 1D direction.

shown in Fig. 6 for a momentum transfer of 0.1 Å^{-1} along the 1D direction. The original loss spectrum was measured in a wide energy range between 0.2 and 95.2 eV to avoid inaccuracy due to too severe assumptions concerning the extrapolation for $\omega\rightarrow\infty$ and was corrected for finite momentum resolution and multiple-scattering contributions. The contribution of the direct beam was eliminated by fitting the plasmon peak as described above, which thereby gives the low-energy tail to zero energy for the loss function. The scaling for the loss function was achieved through $\mathrm{Re}(1/\varepsilon)=0$ for $\omega\rightarrow 0$ from the condition for a metallic material. The legitimacy of the corrections made was checked by a comparison of the reflectance as calculated from ε_1 and ε_2 with that from our optical measurements (not shown). The onset of strong interband transitions can be seen from ε_2 to lie at about 2.7 eV, which is far above the energy of the plasmon excitation so that we do not need to consider them further. To reveal the relative oscillator strength of the weak $\pi^*\rightarrow\pi^*$ interband transitions we proceed as follows. From ε_2 we get the optical conductivity through $\sigma_1(\omega)=\varepsilon_0\omega\varepsilon_2(\omega)$, where contrary to the loss function the Drude part and the contributions of the Lorentz oscillators enter additively. We then fit the optical conductivity using the Drude term and a large number of Lorentzians. We stress that we do not assign a specific physical meaning to the individual Lorentz oscillators: they merely serve as reasonable fit functions fulfilling the *f*-sum rule as a minimal physical side condition. Since the optical conductivity is finite for zero energy, this gives a more accurate fit of the Drude part than is the case for ε_2. If one transfers all the ''dummy'' parameters of the Lorentzians into the analogous expression for ε_1, omitting the Drude term, one ends up with a function depicted in Fig. 7, which represents ε_1 *without* the Drude part $-\omega_p^2/(\Gamma^2+\omega^2)$, where Γ is the plasmon damping constant. One can now judge at a glance that the oscillator strength of the $\pi^*\rightarrow\pi^*$ interband transitions (marked by the arrow in Fig. 7) is truly low and derive a value for the background dielectric constant $\varepsilon_\infty=5.7$, which has now turned out indeed to be a meaningful quantity.

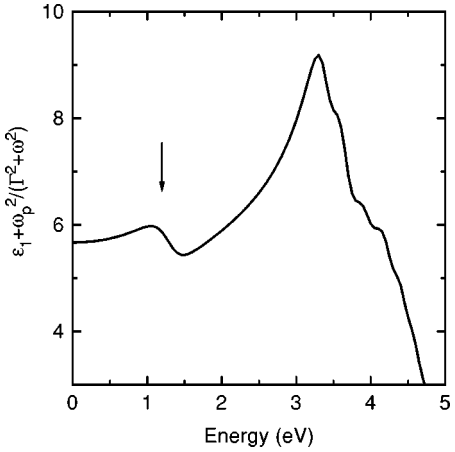

FIG. 7. The real part ε_1 of the dielectric function without the Drude contribution, $-\omega_p^2/(\Gamma^2+\omega^2)$, for the 1D direction ($q=0.1$ Å^{-1}). For details see the text.

Thus, we now switch back to the comparison between theory and experiment and note that one cannot directly apply Eqs. (4) and (5) because even the smallest measured momentum transfer is significantly far from the long-wavelength limit upon considering the Fermi wave number $k_F=0.31$ Å^{-1}. Therefore, we first fitted the experimental data (see Fig. 8) in the interval $0\leqslant q_z\leqslant 0.3$ Å^{-1} with polynomials of fourth order, i.e., $\omega(q_z)=\omega_p+Aq_z^2+Bq_z^4$, and sixth order, i.e., $\omega(q_z)=\omega_p+Aq_z^2+Bq_z^4+Cq_z^6$. The values of the plasma frequency and the dispersion coefficient A obtained hardly differ between the fourth- and sixth-order fits. Thus, we achieved convergence for ω_p and A with the polynomial of sixth order, giving values of $\omega_p=1.5$ eV and $A=3.6$ eV Å^2. With these values and by using the theoretical formulas (4) and (5) one can then obtain figures for the background dielectric constant and the hopping integral, viz $\varepsilon_\infty=4.8$ and $t=0.5$ eV. From optical reflectance measurements a screened plasma frequency of 1.35 eV was found, which gives, by means of a decoupling procedure involving a KKA, an unscreened plasma frequency of 2.7 eV.[56] Comparing these two values, one arrives at a dielectric constant of about 4 in comparison to the value of 5.7 from the analysis of the EELS data above. Thus, the values of $\omega_p=1.5$ eV and ε_∞

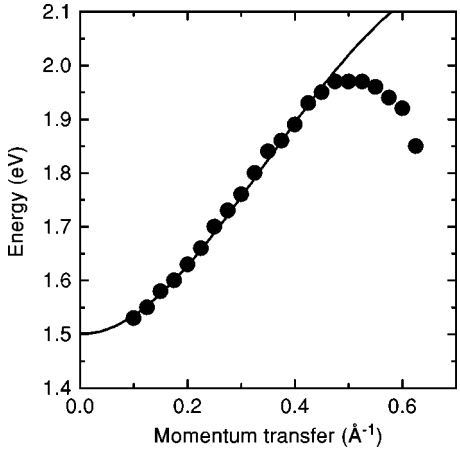

FIG. 8. Experimental (dots) and theoretical (line) plasmon dispersion along the 1D direction for $K_{0.3}MoO_3$.

$=4.8$ obtained from the plasmon dispersion fit in quite well. The same holds for the conduction-band width A (see Fig. 2), which comes out to be $2t=1$ eV, which is in good comparison with the values reported for photoemission measurements[58] and with the TB calculations of Travaglini and Wachter.[53]

Finally, with the values for t and ε_∞ and by means of Eq. (2), the theoretical plasmon dispersion can be deduced. The results for $\omega(q_z)$ are plotted in Fig. 8 (solid line) together with the experimental data for the plasmon peak positions (dots) derived from the same fits that were used to deduce the plasmon widths. The agreement between theory and experiment is excellent up to a momentum transfer of $q \approx 0.42$ Å^{-1}, which covers the quasilinear part of the dispersion. However, there is a large deviation for $q_z > 0.42$ Å^{-1}. This we assign mainly to the crystal local-field effects according to the discussion in Sec. III B, but also other causes such as additional band-structure effects or an enhanced damping may contribute to the bending down of the dispersion curve at higher momentum transfers.

From the foregoing discussion the important message is that a quantitative description of the quasilinear part of the plasmon dispersion along the 1D axis can be achieved remaining in the framework of the RPA. Not surprisingly, crystal local-field effects become important at higher momentum transfers leading to a bending down of the dispersion curve. Modifications due to corrections going beyond the RPA are expected to be small.

B. Angular dependence of the plasmon excitations

Before we discuss our experimental results regarding the angular dependence of the plasmon excitations, we want to refresh the reader's memory regarding some remarks made in the Introduction about the different theoretical predictions in this context. The central difference in the conclusions of the various RPA-based theories concerns the energy of the plasmon excitations perpendicular to the chains, and originates solely from the level at which they treat the coupling between the 1D chains. If besides the interchain Coulomb interaction an additional coupling through a transverse electron hopping $t_\perp$ is forbidden, an angular dependence given by $\cos(\theta)$ is expected in the long-wavelength limit,[32,36–39] whereas for $t_\perp \neq 0$ the plasmon energy remains finite even for $\theta=90°$.[30] This statement holds irrespective of any corrections for exchange and/or correlation. Also, in a LL-based description the $\cos(\theta)$ angular dependence of the plasmon energy for $q \to 0$ is valid in the case of a zero transverse hopping probability.[10,40] A LL treatment extended to finite $t_\perp$ and finite momentum transfers, however, is nontrivial and has still to be done.

The angular dependence of the plasmon excitations is illustrated for the two most instructive examples in Figs. 9 and 10. Here the loss functions, normalized in the same way as described earlier, are shown as a function of momentum transfer for a fixed angle $\theta=90°$ (Fig. 9) and, vice versa, as a function of the angle relative to the 1D direction for a fixed momentum transfer $q=0.35$ Å^{-1} (Fig. 10). Going to higher momentum transfers, the striking feature in Fig. 9 is a splitting of the single peak, situated at 1.35 eV for $q=0.1$ Å^{-1}. We point out that this energy position of 1.35 eV is only slightly below the value of 1.53 eV for the plasmon peak at the same momentum transfer for $\theta=0°$, which is in contradiction to what one would expect from the existing model calculations.

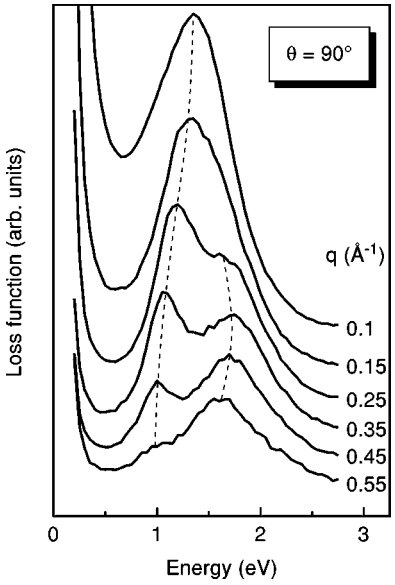

FIG. 9. Normalized electron energy-loss spectra for different momentum transfers perpendicular to the 1D direction (i.e., at $\theta=90°$). The dashed lines are intended as a guide to the eye.

If one traces the evolution of this single peak with increasing momentum transfer one is led to identify the low-energy structure, which continuously loses spectral weight with growing q, with one peak, while one recognizes a second peak emerging with larger q at higher energy. Looking at Fig. 10 where a similar splitting is observed one may similarly argue that starting at $\theta=0°$ one can follow the plasmon mode, which was identified unambiguously in Sec. IV A, throughout the whole angle range between 0° and 90°.

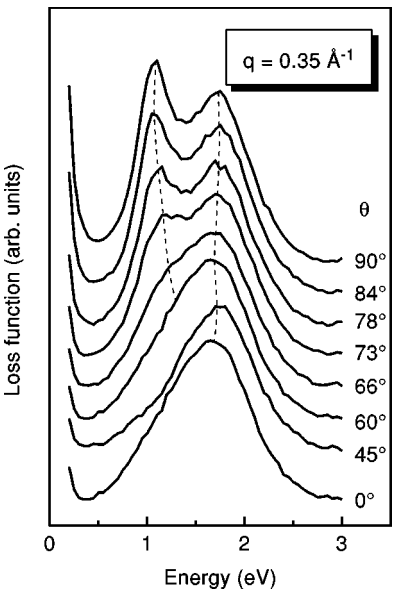

FIG. 10. Normalized electron energy-loss spectra for a fixed momentum transfer of $q=0.35$ Å^{-1} recorded at different angles θ relative to the 1D direction. The dashed lines are intended as a guide to the eye.

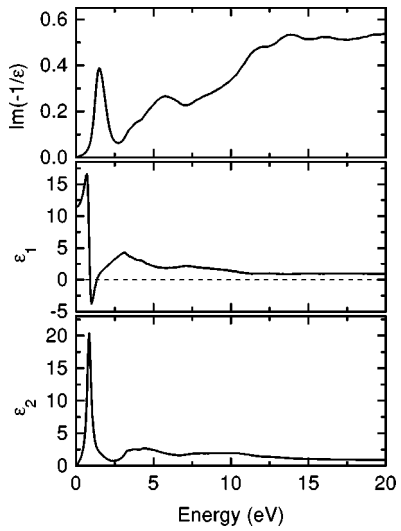

FIG. 11. The loss function $\mathrm{Im}(-1/\varepsilon)$ and the real (ε_1) and imaginary part (ε_2) of the dielectric function of $K_{0.3}MoO_3$ for a momentum transfer of $q=0.1$ Å^{-1} perpendicular to the 1D direction.

Doing this one arrives at an assignment of the higher energy structure to the plasmon excitation. Since the splitting occurs in an angle range where the component of the momentum transfer perpendicular to the 1D axis hardly changes, an effect due to a dimensional crossover can be excluded. Turning back to Fig. 9 one then has to ascribe the low-energy structure to the $\pi^*\rightarrow\pi^*$ interband transitions and the high-energy structure to the plasmon mode, which is no longer discernible for small q and $\theta=90°$. This interpretation is supported by the reflectance measurements where with the polarization vector perpendicular to the chain direction a semiconducting rather than a metallic behavior is observed. A KKA of the EELS data for $\theta=90°$ and $q=0.1$ Å^{-1} reveals the situation more clearly (see Fig. 11). Besides the usual corrections and precautions as addressed above, the elastic line was eliminated simply so as to achieve good agreement with the reflectance from the optical measurements. The scaling condition $\varepsilon_1(\omega=0)=11.5$ was used as derived from the reflectance through $\varepsilon_1(0)=n(0)^2=[(1+\sqrt{R(0)})/(1-\sqrt{R(0)})]^2$ for a nonmetallic, nonmagnetic solid. In ε_2 a strong oscillator is found at 1.5 eV, which is consistent with the assumption of a strongly increased strength of the $\pi^*\rightarrow\pi^*$ interband transitions compared to the chain direction. The oscillator strength is even high enough such that a zero crossing occurs in ε_1, giving rise to a peak in the loss function, which is therefore called an *interband* plasmon. Similar to the case of the 1D direction, the onset of the next higher interband transitions, as is clear from ε_2, is far above this interband plasmon energy of about 2.8 eV, and hence need not be considered further. However, the fact that the character of the plasmon excitation alters for a momentum transfer $q=0.1$ Å^{-1} between the two perpendicular directions without any sign of a significant peak broadening or splitting (also for intermediate angles that are not shown) suggests a more subtle picture. The complex interplay between the intraband and $\pi^*\rightarrow\pi^*$ interband transitions, which strongly depends on the momentum transfer **q**, i.e., from both its modulus and its angle, leads not only to a mutual repulsion of the energetically close-lying (charge-carrier) plasmon and the interband transitions but also to a change of the character of the plasmon mode itself, making the identification of the observed structures in the loss function with a particular type of excitation impossible. This fact explains the above-mentioned discrepancy with the theoretical predictions.

Finally, to build a bridge to the discussion in Sec. III A, we note that the splitting of the plasmon-related peak in the loss function can qualitatively also be understood from the fact that for momentum transfers with components $\neq 0$ not only in the z direction, transitions involving band C are not longer forbidden due to symmetry. This means that there are then two types of electronic transitions contributing to the dielectric function in the same energy region, which may lead to two plasmon branches depending on the subtleties of the behavior of the relevant matrix elements as a function of **q**.

V. SUMMARY

We have shown that in the blue bronze $K_{0.3}MoO_3$ the quasilinear part of the plasmon dispersion along the 1D axis can be described excellently within the framework of the RPA using the Ehrenreich-Cohen formula. In the momentum range up to $q\approx 0.42$ Å^{-1} we isolate as the leading contributions to the dispersion coefficient a proper treatment of the real electronic transitions and the inclusion of the effects originating from the variation of the reciprocal dynamic effective mass. For larger momentum transfers $q>0.42$ Å^{-1}, in particular, the crystal local-field effects become important and the theoretically determined plasmon-dispersion curve no longer describes the experimental one. Nevertheless, at no stage is there a hint for the need of corrections due to exchange and correlation, or for a Luttinger liquid-based description. Our combined experimental and theoretical investigation rather corroborates previous band-structure calculations by Travaglini and Wachter. Unfortunately, the experimental results gained by varying the plasmon propagation angle relative to the chain axis give a distorted picture owing to interband transitions. The latter are strong for propagation directions away from the 1D axis, and hence strongly affect the plasmon modes in these directions. Thus, a comparison with the existing theories is not possible.

ACKNOWLEDGMENTS

We thank D. Stephan and K. Widder for characterization of the crystals and are grateful to S.-L. Drechsler and R. Claessen for fruitful discussions. We thank M.S. Golden for a critical reading of the manuscript. V.G.G. and G.P. gratefully acknowledge financial support by the Deutsche Forschungsgemeinschaft (DFG).

APPENDIX A: ALLOWED AND FORBIDDEN ELECTRONIC TRANSITIONS FOR THE $K_{0.3}MoO_3$ MODEL SPECTRUM

In the following we give proof that normal interband transitions $A\rightarrow B$ and umklapp intraband transitions $A\rightarrow A$ are forbidden for the model spectrum established in Eqs. (1) because of its folded structure. On the other hand, we will see

that umklapp interband transitions $A \rightarrow B$ and normal intraband transitions $A \rightarrow A$ are allowed. These facts are illustrated in Fig. 3(a), where the bands A and B are drawn within the repeated-zone scheme. The first and the second BZ's are depicted. Allowed and forbidden transitions are marked exemplarily by solid and dotted arrows, respectively. Figure 3(b) shows the same band structure within the extended-zone scheme. It is easily seen that the band A in the first and the band B in the second BZ from Fig. 3(a) coincide with the band A_0 in Fig. 3(b). We will distinguish two regions in the first BZ, the region ''I'' with $-\pi/b \leqslant k_z < 0$, and the region ''II'' with $0 \leqslant k_z < \pi/b$. If the energy-momentum relation for band A is denoted by $E^A_{k_z}$, the dispersion relation for band B $E^B_{k_z}$ can be expressed as $E^A_{k_z+b^*}$ in region ''1'' and $E^A_{k_z-b^*}$ in region ''2'' or expressed in terms of the Bloch amplitudes of the bands A and B

$$u^B_{k_z}(z) = \begin{cases} u^A_{k_z+b^*}(z) & \text{for} \quad -\pi/b \leqslant k_z < 0 \\ u^A_{k_z-b^*}(z) & \text{for} \quad 0 \leqslant k_z < \pi/b. \end{cases} \tag{A1}$$

If one combines Eq. (A1) with

$$u_{\mathbf{k}}(\mathbf{r}) = e^{i\mathbf{G}\mathbf{r}} u_{\mathbf{k}+\mathbf{G}}(\mathbf{r}), \tag{A2}$$

which is a simple consequence of Bloch's theorem—$\mathbf{k}$ lies in the first BZ and $\mathbf{G}$ is a reciprocal lattice vector—Eq. (A1) becomes

$$u^B_{k_z}(z) = \begin{cases} e^{-ib^*z} u^A_{k_z}(z) & \text{for} \quad -\pi/b \leqslant k_z < 0 \\ e^{+ib^*z} u^A_{k_z}(z) & \text{for} \quad 0 \leqslant k_z < \pi/b. \end{cases} \tag{A3}$$

The typical integral in the dielectric function, which describes the intensity of the interband transitions $A \rightarrow B$ is of the form[63]

$$I_n = \int_0^b dz [u^B_{k_z+q_z+nb^*}(z)]^* u^A_{k_z}(z). \tag{A4}$$

In Eq. (A4) both k_z and $k_z+q_z+nb^*$ lie in the first BZ. Thus, for $n=0$ one has normal processes and for $n \neq 0$ umklapp processes. For simplicity we will assume $q_z > 0$ and, additionally, for umklapp processes $n=-1$.

First we consider normal processes $A \rightarrow B$. Replacing in the integrand of (A4) the Bloch amplitude of the band B according to (A3) one obtains after a simple transformation

$$\begin{aligned} I_0 &= \int_0^{b/2} dz e^{\pm ib^*z} [u^A_{k_z+q_z}(z)]^* u^A_{k_z}(z) \\ &\quad + \int_{b/2}^{b} dz e^{\pm ib^*z} [u^A_{k_z+q_z}(z)]^* u^A_{k_z}(z) \\ &= \int_0^{b/2} dz [1 + e^{\mp ib^* b/2}] e^{\pm ib^*z} [u^A_{k_z+q_z}(z)]^* u^A_{k_z}(z) = 0, \end{aligned} \tag{A5}$$

which states that the normal interband transitions $A \rightarrow B$ are forbidden since k_z+q_z lies in the second BZ. In obtaining (A5) we used that $u^A_{k_z}(z) = u^{A_0}_{k_z}(z)$ in the first BZ of Fig. 3(a) and the periodic properties of the Bloch amplitude of the band A_0, $u^{A_0}_{k_z}(z \pm b/2) = u^{A_0}_{k_z}(z)$.

The analogous consideration for the umklapp processes $A \rightarrow B$ gives the result

$$\begin{aligned} I_{-1} &= 2 \int_0^{b/2} dz [u^B_{k_z+q_z}(z)]^* u^A_{k_z}(z) \\ &= 2 \int_0^{b/2} dz [u^{A_0}_{k_z+q_z}(z)]^* u^{A_0}_{k_z}(z), \end{aligned} \tag{A6}$$

using $u^B_{k_z+q_z}(z) = u^{A_0}_{k_z+q_z}(z)$. In this case the integral does not vanish *a priori* and its value depends on the symmetrical properties of the Bloch amplitude $u^{A_0}_{k_z}(z)$. Equation (A6) shows that umklapp interband processes $A \rightarrow B$ appear in the extended band scheme as normal intraband processes $A_0 \rightarrow A_0$. One can similarly check that umklapp intraband processes $A \rightarrow A$ are forbidden as well.

To summarize the above discussion, in order to account for all the real electronic transitions one can carry out the calculations simply in the extended zone scheme with the zone boundaries at $\pm 2b^* = \pm 0.84$ Å^{-1}. One thereby has to consider only normal intraband electronic transitions within the band A_0,

$$E_{k_z} := E^{A_0}_{k_z} = 2t[1 - \cos(k_z b/2)]. \tag{A7}$$

APPENDIX B: LONG-WAVELENGTH EXPANSION OF THE PLASMON DISPERSION AND RESULTS FOR $K_{0.3}MoO_3$

In the following we give a brief outline of the reasoning leading from the Ehrenreich-Cohen formula for the dielectric function (2) to the expressions (4) and (5), which apply to the blue bronze and enter the general Eq. (3) for the long-wavelength expansion of the plasmon dispersion.

The tensorial $\mathbf{q}$ expansion of the integrand in Eq. (2) up to the fourth order and integration by parts exploiting inversion symmetry yields to an integral expression, which can be transformed into an integral over the Fermi surface according to $\int d^3k \partial/\partial \mathbf{k} = \oint d\mathbf{S}$. This gives, with ε_∞ included, the long-wavelength expansion for the dielectric function as stated by Nücker *et al.*:[64]

$$\begin{aligned} \varepsilon_1(\mathbf{q},\omega) &= \varepsilon_\infty - \frac{4\pi e^2}{\omega^2} \\ &\quad \times \left\{ \langle v_q^2 \rangle + q^2 \left[\frac{\langle v_q^4 \rangle}{\omega^2} + \frac{1}{12} \left\langle v_q \left(\mathbf{e} \frac{\partial}{\partial \mathbf{k}} \right)^2 v_q \right\rangle \right] \right\}, \end{aligned} \tag{B1}$$

where v_q is the projection of the quasiclassical velocity onto the plasmon propagation direction according to

$$v_q = \mathbf{e} \cdot \mathbf{v}, \quad \mathbf{e} = \mathbf{q}/q, \quad \mathbf{v} = \frac{1}{\hbar} \frac{\partial E_{\mathbf{k}}}{\partial \mathbf{k}}, \tag{B2}$$

and the brackets denote a Fermi-surface integral defined as

$$\langle H\rangle = \frac{2}{(2\pi)^3}\int d^3k[-f'(E_{\mathbf{k}})]H(\mathbf{k},\mathbf{q}) = \frac{2}{(2\pi)^3}\int_{E_{\mathbf{k}}=E_F}\frac{dS}{\hbar|\mathbf{v}|}H(\mathbf{k},\mathbf{q}), \tag{B3}$$

where $-f'(E_{\mathbf{k}}) = -(\partial f(E_{\mathbf{k}})/\partial E_{\mathbf{k}}) = \delta(E_F - E_{\mathbf{k}})$. Equation (2), which determines approximately the plasmon dispersion, yields with the expansion (B1) a biquadratic equation for the plasmon frequency. The solution up to q^2 gives the dispersion relation within the long-wavelength limit as

$$\omega(\mathbf{q}) = \omega_p + Aq^2, \quad A = \frac{\hbar}{m}\alpha, \quad \omega_p^2 = \frac{4\pi e^2}{\varepsilon_\infty}\frac{n}{m_{opt}}, \quad \frac{n}{m_{opt}} = \langle v_q^2\rangle, \tag{B4}$$

with the free-electron mass m. The optical effective mass is defined by the third equation. The dispersion coefficient takes the form

$$\alpha = \frac{m}{2\hbar}\frac{1}{\omega_p}\left\{\frac{\langle v_q^4\rangle}{\langle v_q^2\rangle} + \frac{1}{12}\frac{4\pi e^2}{\varepsilon_\infty}\left\langle v_q\left|\left(\mathbf{e}\frac{\partial}{\partial\mathbf{k}}\right)^2 v_q\right\rangle\right\}\right\} \equiv \alpha_1 + \alpha_2. \tag{B5}$$

*Present address: Gesellschaft für Schwerionenforschung mbH, Planckstr. 1, D-64291 Darmstadt, Germany.

[1] L. D. Landau, Zh. Éksp. Teor. Fiz. **30**, 1058 (1956) [Sov. Phys. JETP **3**, 920 (1956)]; **32**, 59 (1957) [**5**, 101 (1957)].

[2] P. Nozières and D. Pines, *The Theory of Quantum Liquids* (Addison-Wesley, Redwood City, CA, 1994).

[3] M. J. Graf, D. Rainer, and J. A. Sauls, Phys. Rev. B **47**, 12 089 (1993).

[4] P. W. Anderson, Phys. Rev. Lett. **64**, 1839 (1990); **65**, 2306 (1990); Science **256**, 1526 (1992).

[5] R. E. Peierls, *Quantum Theory of Solids* (Clarendon Press, Oxford, 1955).

[6] S. Tomonaga, Prog. Theor. Phys. **5**, 349 (1950).

[7] J. M. Luttinger, J. Math. Phys. **4**, 1154 (1963).

[8] D. C. Mattis and E. H. Lieb, J. Math. Phys. **6**, 304 (1965).

[9] F. D. M. Haldane, J. Phys. C **14**, 2585 (1981).

[10] For a review see J. Voit, Rep. Prog. Phys. **57**, 977 (1994).

[11] See, for instance, G. Grüner, in *Density Waves in Solids*, edited by D. Pines, Frontiers in Physics Vol. 89 (Addison-Wesley, Reading, MA, 1994), and references therein.

[12] B. Dardel, D. Malterre, M. Grioni, P. Weibel, Y. Baer, and F. Lévy, Phys. Rev. Lett. **67**, 3144 (1991).

[13] Y. Hwu, P. Alméras, M. Marsi, H. Berger, F. Lévy, M. Grioni, D. Malterre, and G. Margaritondo, Phys. Rev. B **46**, 13 624 (1992).

[14] C. Coluzza, H. Berger, P. Alméras, F. Gozzo, G. Margaritondo, G. Indlekofer, L. Forro, and Y. Hwu, Phys. Rev. B **47**, 6625 (1993).

[15] G.-H. Gweon, J. W. Allen, R. Claessen, J. A. Clack, D. M. Poirier, P. J. Benning, C. G. Olson, W. P. Ellis, Y.-X. Zhang, L. F. Schneemeyer, J. Marcus, and C. Schlenker, J. Phys.: Condens. Matter **96**, 9923 (1996).

[16] B. Dardel, D. Malterre, M. Grioni, P. Weibel, Y. Baer, J. Voit, and D. Jérôme, Europhys. Lett. **24**, 687 (1993).

[17] A. Sekiyama, A. Fujimori, S. Aonuma, H. Sawa, and R. Kato, Phys. Rev. B **51**, 13 899 (1995).

[18] T. Takahashi, T. Yokoya, A. Chainani, H. Kumigashira, O. Akaki, and R. Kato, Phys. Rev. B **53**, 1790 (1996).

[19] F. Zwick, S. Brown, G. Margaritondo, C. Merlic, M. Onellion, J. Voit, and M. Grioni, Phys. Rev. Lett. **79**, 3982 (1997).

[20] V. Meden and K. Schönhammer, Phys. Rev. B **46**, 15 753 (1992).

[21] J. Voit, Phys. Rev. B **47**, 6740 (1993); J. Phys.: Condens. Matter **5**, 8305 (1993); Synth. Met. **70**, 1015 (1995); J. Phys.: Condens. Matter **8**, L779 (1996).

[22] K. Schönhammer and V. Meden, Phys. Rev. B **47**, 16 205 (1993); J. Electron Spectrosc. Relat. Phenom. **62**, 225 (1993); Phys. Rev. B **48**, 11 390 (1993).

[23] V. Meden, K. Schönhammer, and O. Gunnarsson, Phys. Rev. B **50**, 11 179 (1994).

[24] P. Kopietz, V. Meden, and K. Schönhammer, Phys. Rev. Lett. **74**, 2997 (1995).

[25] W. Brütting, P. H. Nguyen, W. Rieß, and G. Paasch, Phys. Rev. B **51**, 9533 (1995).

[26] W. Brütting, W. Rieß, P.H. Nguyen, and G. Paasch, in *The Physics of Semiconductors*, edited by M. Scheffler and R. Zimmermann (World Scientific, Singapore, 1996), Vol. 4, p. 3363.

[27] J. J. Ritsko, D. J. Sandman, A. J. Epstein, P. C. Gibbons, S. E. Schnatterly, and J. Fields, Phys. Rev. Lett. **34**, 1330 (1975).

[28] C. H. Chen, J. Silcox, A. F. Garito, A. J. Heeger, and A. G. MacDiarmid, Phys. Rev. Lett. **36**, 525 (1976).

[29] M. Sing, V. G. Grigoryan, G. Paasch, M. Knupfer, J. Fink, H. Berger, and F. Lévy, Phys. Rev. B **57**, 12 768 (1998).

[30] H. L. Cui, X. J. Lu, N. J. M. Horing, and X. L. Lei, Phys. Rev. B **40**, 3443 (1989).

[31] P. F. Williams and A. N. Bloch, Phys. Rev. Lett. **36**, 64 (1976).

[32] L. M. Kahn, J. Ruvalds, and R. Hastings, Phys. Rev. B **17**, 4600 (1978).

[33] K. Kaneto, Y. Yoshino, and Y. Inuishi, in *Electronic Properties of Inorganic Quasi-One-Dimensional Compounds*, edited by P. Monceau (Reidel, Dordrecht, 1985), Pt. II, and references therein.

[34] J. Bernasconi, P. Brüesch, D. Kuse, and H. R. Zeller, J. Phys. Chem. Solids **35**, 145 (1974).

[35] C. S. Jacobsen, D. B. Tanner, A. F. Garito, and A. J. Heeger, Phys. Rev. Lett. **33**, 1559 (1974).

[36] P. F. Williams and A. N. Bloch, Phys. Rev. B **10**, 1097 (1974).

[37] A. Nobile and E. Tosatti, J. Phys. C **13**, 589 (1980).

[38] F. Brosens, J. T. Devreese, L. M. Kahn, and J. Ruvalds, Phys. Status Solidi B **111**, 95 (1982).

[39] I. E. Dzyaloshinskii and E. I. Kats, Zh. Éksp. Teor. Fiz. **55**, 338 (1968) [Sov. Phys. JETP **28**, 178 (1969)].

[40] H. J. Schulz, J. Phys. C **16**, 6769 (1983).

[41] H. J. Schulz, Phys. Rev. Lett. **71**, 1864 (1993).

[42] A. Wold, W. Kunnmann, R. J. Arnott, and A. Ferretti, Inorg. Chem. **3**, 545 (1964); B. Lommel, diploma thesis, Universität Frankfurt, 1988.

[43] J. Graham and A. D. Wadsley, Acta Crystallogr. **20**, 93 (1966).

[44] R. M. Fleming, L. F. Schneemeyer, and D. E. Moncton, Phys. Rev. B **31**, 899 (1985).

[45] Further on we denote the crystallographic *b* axis as the *z* direction.

[46] C. Schlenker and J. Dumas, in *Crystal Chemistry and Properties of Materials with Quasi-One-Dimensional Structures*, edited by

J. Rouxel (Reidel, Dordrecht, 1986), p. 135.
[47] J. Fink, Adv. Electron. Electron Phys. **75**, 121 (1989).
[48] Q. P. Li, S. Das Sarma, and R. Joynt, Phys. Rev. B **45**, 13 713 (1992).
[49] S. Das Sarma and E. H. Hwang, Phys. Rev. B **54**, 1936 (1996).
[50] R. Liebmann, P. Lemke, and J. Appel, Phys. Rev. B **16**, 4230 (1977).
[51] L. Calmels and A. Gold, Phys. Rev. B **52**, 10 841 (1995).
[52] V. B. Campos, O. Hipólito, and R. Lobo, Phys. Status Solidi B **81**, 657 (1977).
[53] G. Travaglini and P. Wachter, in *Charge Density Waves in Solids*, edited by G. Hutiray, Lecture Notes in Physics Vol. 217 (Springer, Berlin, 1985), p. 115.
[54] M.-H. Whangbo and L. F. Schneemeyer, Inorg. Chem. **25**, 2424 (1986).
[55] G. Travaglini and P. Wachter, J. Phys. Soc. Jpn. Suppl. A **49**, 869 (1980).
[56] G. Travaglini, P. Wachter, J. Marcus, and C. Schlenker, Solid State Commun. **37**, 599 (1981).
[57] G. K. Wertheim, L. F. Schneemeyer, and D. N. E. Buchanan, Phys. Rev. B **32**, 3568 (1985).
[58] R. Claessen, G.-H. Gweon, F. Reinert, J. W. Allen, W. P. Ellis, Z. X. Shen, C. G. Olson, L. F. Schneemeyer, and F. Lévy, J. Electron Spectrosc. Relat. Phenom. **76**, 121 (1995).
[59] M. Sing, R. Neudert, H. von Lips, M. S. Golden, M. Knupfer, J. Fink, R. Claessen, J. Mücke, H. Schmitt, S. Hüfner, B. Lommel, and W. Aßmus (unpublished).
[60] H. Ehrenreich and M. H. Cohen, Phys. Rev. **115**, 786 (1959).
[61] G. Paasch and V. G. Grigoryan (unpublished).
[62] A. vom Felde, J. Sprösser-Prou, and J. Fink, Phys. Rev. B **40**, 10 181 (1989).
[63] W. M. Saslow and G. F. Reiter, Phys. Rev. B **7**, 2995 (1973).
[64] N. Nücker, U. Eckern, J. Fink, and P. Müller, Phys. Rev. B **44**, 7155 (1991).